Mutual Solubility of Water and Structural/Positional Isomers of *N*-Alkylpyridinium-Based Ionic Liquids

Mara G. Freire,[†,‡] Catarina M. S. S. Neves,[‡] Karina Shimizu,[§] Carlos E. S. Bernardes,[§] Isabel M. Marrucho,[†] João A. P. Coutinho,[‡] José N. Canongia Lopes,*[,†,§] and Luís Paulo N. Rebelo*[,†]

Instituto de Tecnología Química e Biológica, UNL, Av. República 127, 2780-901 Oeiras, Portugal, CICECO, Departamento de Química, Universidade de Aveiro, 3810-193 Aveiro, Portugal, and Centro de Química Estrutural, Instituto Superior Técnico, UTL, 1049 001 Lisboa, Portugal

Received: September 30, 2010; Revised Manuscript Received: October 21, 2010

Despite many previous important contributions to the characterization of the liquid−liquid phase behavior of ionic liquids (ILs) plus water systems, a gap still exists as far as the effect of isomers (of ILs) is concerned. Therefore, in this work, a comprehensive study of the liquid−liquid equilibria between water and isomeric pyridinium-based ionic liquids has been performed. Atmospheric pressure mutual solubilities between water and pyridinium-based ionic liquids combined with the common anion bis[(trifluoromethyl)sulfonyl]imide were experimentally determined between (288.15 and 318.15) K. The main goal of this work is to study the isomeric effects on the pyridinium-based cation, namely, the structural and positional isomerism, as well as the alkyl side chain length. To the best of our knowledge, the influence of both structural and positional isomerism on the liquid−liquid behavior in ionic-liquid-water-containing systems is an unexplored field and is here assessed for the first time. Moreover, from the experimental solubility data, several infinite dilution molar thermodynamic functions of solution, namely, the Gibbs energy, the enthalpy, and the entropy, were estimated and discussed. In addition, aiming at gathering a broader picture of the underlying thermodynamic solvation phenomenon, molecular dynamics simulations were also carried out for the same experimental systems.

Introduction

The term ionic liquid (IL) has come up to define a novel class of fluids entirely composed of ions which present melting points below a conventional temperature of 373 K.[1] Numerous promising applications in industry have pointed to this type of chemical, such as alternatives to the currently used volatile organic solvents, among others. Some of their remarkable properties, such as negligible vapor pressure at ambient conditions,[2] broad liquid temperature range, and high specific solvent quality, have prompted an increased interest from both the industrial and academic communities. Furthermore, the wide array of possible cation−anion combinations permits a significant flexibility in designing new ionic fluids and in optimizing their physical/chemical properties for particular applications, and thus, ionic liquids are generally referred to as "designer solvents". Nevertheless, due to their ionic nature, ionic liquids are highly complex fluids when compared to single molecular solvents. Consequently, a molecular-based understanding of the ionic liquid solution behavior is a challenging task because their electrical charges, polarity, and molecular and electronic structure result in a multifaceted combination of specific interactions (Coulombic, van der Waals, hydrogen-bonding, and $\pi\cdots\pi$ interactions). Even so, among all the interactions taking place in ionic liquids, Coulombic interactions are predominant, culminating therefore in an increase of the ionic liquids' cohesive energy.[3,4]

A meticulous feature of ionic liquids—one in which imidazolium-based ionic liquids have thoroughly been investigated—is the possibility of tailoring their amphiphilic character and their hydrophobicity by simple variation of the alkyl side chain length.[5] Indeed, diffraction studies[6,7] have shown noticeable molecular organization of ionic liquids at the nanometer scale, while molecular simulation studies[8,9] have revealed that imidazolium-based ionic liquids with side chains greater than that of butyl exist as microstructured neat fluids. This local structure network of ionic liquids, with nonpolar domains formed by alkyl chains, and concomitantly ionic domains composed of charged parts, grants ionic liquids with a dual nature[10] of their liquid state. This tendency of nanoscale segregation is not only evident in pure ionic liquids but also is extended to their aqueous solutions. In this context, and aiming at understanding the interactions between ionic liquids and water, both experimental[5,11−23] and theoretical[18,24−26] investigations have been carried out. Experimental techniques comprised IR and Raman spectroscopy,[11−14] NMR spectroscopy,[15−19] SFG spectroscopy,[20] and X-ray crystallography,[21] among others.[22,23] A key aspect which has derived from such studies is that the aggregation of ILs in aqueous solutions largely depends on their concentration regimes. For instance, thermodynamic approaches on imidazolium-based ionic liquids and water binary systems have shown that only below a mole fraction of ionic liquid in the order of 0.013−0.015 the cation and counterion are completely dissociated.[22] At higher mole fractions, above that threshold, ions begin to interact and organize themselves by mutual attraction forces.[22] On the contrary, at the IL-rich solution side, it has been reported that water molecules influence the environment of both ionic liquids, cation and anion, weakening their cohesion forces.[22] Indeed, at high ionic liquid contents, $x_{IL} > 0.5-0.6$, ionic liquid

* Corresponding authors. E-mail: jnlopes@ist.utl.pt; luis.rebelo@itqb.unl.pt.
† ITQB-UNL (www.itqb.unl.pt).
‡ Universidade de Aveiro (www.ciceco.ua.pt).
§ UTL (cqe.ist.utl.pt).

10.1021/jp1093788
Published on Web 11/15/2010

ions form clusters while water molecules interact with them, without forming a hydrogen-bonding network among themselves.[22] Therefore, the network structure of ionic liquids is still preserved when small amounts of water are present.[14] There is thus a critical mole fraction turnover where ion−ion, ion−water−ion, or water−water interactions become dominant.

A strategy combining both experimental measurements and molecular modeling studies can improve our knowledge on fundamental aspects underlying thermodynamic phenomena, such as solubility behavior and phase equilibrium. Despite the growing interest in ionic liquids, accurate experimental data for the liquid−liquid behavior between ionic liquids and water are limited[27−45] or even absent for some classes of ionic liquids. Moreover, the use of molecular dynamics to understand the solvation of ionic liquids in water or water in ionic liquid media is even scarcer.[18,24−26]

A systematic experimental study of the mutual solubilities between hydrophobic pyridinium-based ionic liquids and water was herein conducted in the temperature range 288.15−318.15 K. The main goal of this work is to evaluate the impact of the structural changes at the ionic liquid cation (with special emphasis on isomeric effects) on their liquid−liquid phase behavior. A similar approach was previously carried out for the liquid−liquid equilibrium of positional isomers of pyridinium-tetrafluoroborate-based ionic liquids and toluene where minor differences in the solubility regimes were found.[46] Nevertheless, in this work, large differences are observed across several quantitative regimes among positional isomers at the IL-rich side. The molecular level issues responsible for the observed solution behavior are discussed based on the analysis of molar solution thermodynamic properties. To gather a broader picture of the underlying mechanism of the ionic liquid and/or water solvation phenomena, molecular simulations have also been performed.

Particularly, we have focused our investigations on pyridinium-based ionic liquids since it has recently been shown that they are generally more environmentally friendly, concerning their biodegradation pathways, than their imidazolium-based counterparts.[47] Moreover, the use of the archetype hydrophobic anion, bis[(trifluoromethyl)sulfonyl]imide, has been revealed to not significantly reduce the biodegradability of such pyridinium-based ionic liquids.[48,49]

Experimental Section

Materials. Experimental liquid−liquid equilibria with water, in the 288.15−318.15 K temperature interval, were studied with the following ionic liquids: 1-butylpyridinium bis[(trifluoromethyl)sulfonyl]imide, $[C_4py][NTf_2]$; 1-hexylpyridinium bis[(trifluoromethyl)sulfonyl]imide, $[C_6py][NTf_2]$; 1-octylpyridinium bis[(trifluoromethyl)sulfonyl]imide, $[C_8py][NTf_2]$; 1-butyl-3-methylpyridinium bis[(trifluoromethyl)sulfonyl]imide, $[C_4\text{-}3\text{-}C_1py][NTf_2]$; and 1-butyl-4-methylpyridinium bis[(trifluoromethyl)-sulfonyl]imide, $[C_4\text{-}4\text{-}C_1py][NTf_2]$. In addition, data reported in the literature[39] for 1-propyl-3-methylpyridinium bis[(trifluoromethyl)sulfonyl]imide, $[C_3\text{-}3\text{-}C_1py][NTf_2]$, were used in this work for comparison purposes. All ionic liquids were purchased from IoLiTec. To reduce the amount of volatile impurities, all samples (circa 10 cm^3) were dried under constant stirring, at moderate temperature (≈353 K) and under moderate vacuum (0.1 Pa), for a minimum of 24 h. After this procedure, the purities of the ILs were further checked by ^1H, ^{13}C, and ^{19}F NMR spectra. All ionic liquids presented mass fraction purities higher than 99%. NMR spectra are provided in the Supporting Information (Part 1). The halide content was quantified by ion chromatography and shown to be inferior to 100×10^{-6} in mass fraction. The cationic structures of the studied ionic liquids and corresponding designations are presented in Figure 1. The water used for the equilibration with each of the ionic liquids was double-distilled, passed through a reverse osmosis system, and finally treated with a Milli-Q plus 185 water purification apparatus. The solvent used on the coulometric Karl Fischer titration was Hydranal-Coulomat AG from Riedel de Haën.

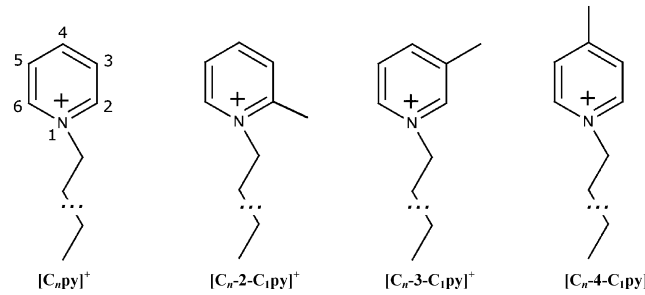

Figure 1. Chemical structure and nomenclature scheme of the several pyridinium-based cations discussed in the present work.

Experimental Procedure. The saturation of both phases was accomplished by mixing water and the respective ionic liquid in excess (approximately 10 cm^3 of each). The two macroscopic separated phases were initially vigorously agitated and allowed to reach the equilibrium for at least 48 h. After this period, all mole fraction solubilities, in both rich phases, have shown to be constant, and thus the equilibrium conditions were attained for all ionic liquids. Temperature was maintained within ±0.01 K using a PID temperature controller driven by a calibrated Pt100 (class 1/10) and by inserting the glass vials containing the two phases at equilibrium in an aluminum block, which in turn is placed inside an isolated air bath. The temperature sensor is inserted directly in the aluminum block embracing the glass vials. Further details about the equilibration conditions and equipment can be found elsewhere.[39−43] The solubility of water in the IL-rich phase was determined by Karl Fischer (KF) titration using a Metrohom 831 KF coulometric titrator, while the solubility of the ionic liquid in the aqueous-rich phase was accomplished by UV spectroscopy with a SHIMADZU UV-1700 Pharma-Spec Spectrometer. Corresponding calibration curves were performed for each ionic liquid at the maximum absorption wavelength and in an adequate concentration range. At least three calibration curves for each ionic liquid were determined to confirm that no gravimetric errors occurred during the stock solution preparation. Both phases were sampled from the equilibrium glass vials using glass syringes maintained dry and at the same temperature of the measurements, avoiding thus phase split or water absorption by temperature variations. All samples were quantified gravimetrically with an uncertainty of the order of $\pm 10^{-5}$ g. The mutual solubility data are the result of an average of at least five independent measurements, i.e., five equilibrated samples.

Molecular Dynamics Simulation Methods. Molecular dynamics (MD) simulations were performed on condensed-phase water/IL mixtures using the DL_POLY program version 2.17.[50] The ionic liquids studied in the MD simulations included 1-butylpyridinium bis[(trifluoromethyl)sulfonyl]imide, $[C_4py][NTf_2]$, and its three (*ortho*, *meta*, and *para*) methyl-substituted derivatives, 1-butyl-2-methylpyridinium bis[(trifluoromethyl)sulfonyl]imide, $[C_4\text{-}2\text{-}C_1py][NTf_2]$, 1-butyl-3-methylpyridinium bis[(trifluoromethyl)sulfonyl]imide, $[C_4\text{-}3\text{-}C_1py][NTf_2]$, and 1-butyl-4-methylpyridinium bis[(trifluoromethyl)sulfonyl]imide, $[C_4\text{-}4\text{-}C_1py][NTf_2]$. The cationic structures of these ILs are depicted in Figure 1. These were modeled using an extended version of

TABLE 1: Solubilities of Water in the IL-Rich Phase (Expressed in Water Mole Fraction, x_w) and of IL in the Water-Rich Phase (Expressed in IL Mole Fraction, x_{IL}) at Different Temperatures[a]

	$[C_4py][NTf_2]$	$[C_6py][NTf_2]$	$[C_8py][NTf_2]$	$[C_3\text{-}3\text{-}C_1py][NTf_2]$[39]	$[C_4\text{-}3\text{-}C_1py][NTf_2]$	$[C_4\text{-}4\text{-}C_1py][NTf_2]$
T/K				x_w		
288.15	0.221(3)	0.204(2)	0.175(3)	0.206(1)	0.190(2)	0.219(1)
293.15	0.238(1)	0.216(1)	0.188(10)	0.226(4)	0.202(1)	0.234(3)
298.15	0.252 (1)	0.225(2)	0.197(10)	0.236(4)	0.213(1)	0.247(3)
303.15	0.269(3)	0.246(3)	0.216(60)	0.260(6)	0.232(2)	0.264(2)
308.15	0.291(1)	0.260(1)	0.234(30)	0.270(3)	0.248(1)	0.285(3)
313.15	0.309(3)	0.277(5)	0.250(10)	0.292(1)	0.261(3)	0.302(2)
318.15	0.327(3)	0.294(1)	0.267(20)	0.310(5)	0.277(1)	0.319(1)
T/K				$10^4 x_{IL}$		
288.15	3.31(2)	1.85(1)	0. 309(1)	3.51(4)	1.99(1)	2.06(2)
293.15	3.39(3)	1.96(2)	0.337(3)	3.66(2)	2.06(1)	2.12(3)
298.15	3.55(5)	2.00(1)	0.350(3)	3.75(2)	2.10(4)	2.21(6)
303.15	3.73(2)	2.07(5)	0.389(4)	3.90(2)	2.18(4)	2.38(3)
308.15	3.98(2)	2.26(8)	0.420(2)	4.27(4)	2.30(5)	2.52(7)
313.15	4.11(1)	2.43(9)	0.446(7)	4.42(4)	2.44(2)	2.62(8)
318.15	4.53(3)	2.56(6)	0.507(9)	4.76(9)	2.54(2)	2.82(7)

[a] The values between parentheses represent the standard deviation associated with the last representative digit.

the CL&P force field.[9] The $[NTf_2]^-$ anion and $[C_npy]^+$ cations had been previously described in the second and third parts of a sequence of articles concerning the application of the CL&P force field to different ionic liquid ions and their homologous series.[51,52] The methyl-substituted $[C_4\text{-}n\text{-}C_1py]^+$ cations were parametrized in the present work taking into account supplementary ab initio calculations at the RHF/6-31G(d) (geometry optimization) and MP2/cc-pVTZ(-f) (electron density calculation) levels using the Gaussian 03 package[53] that yielded new atomic point charges for these cations. All other parameters (bond, angle, dihedral angle, and van der Waals parameters) were taken either from the CL&P[9,49] or the OPLS-aa[54−56] force fields. Water molecules were modeled using the SPC model.[57] All parameters used in the MD calculations are given as Supporting Information (Part 2).

System sizes were chosen to contain about 10 000 atoms, and so, the numbers of cations, anions, and water molecules varied according to the composition of the mixtures. Since these ionic liquids are only partially soluble in water, and most simulations were to be performed under single-phase conditions, two distinct sets of mixtures were considered: $[C_4py]^+$, $[C_4\text{-}n\text{-}C_1py]^+$, and $[NTf_2]^-$ ions at very high dilution in water (1 cation, 1, 3, 10, or 20 ion pairs in 3000 water molecules) and water molecules dissolved in the ionic liquid solvent up to concentrations below the water solubility limit in the ionic liquids (5, 10, 30, and 40 water molecules in 250 ion pairs).

All MD simulation runs were started from low-density configurations, with all ions and water molecules placed at random in period cubic boxes. These were then equilibrated for a period of 0.8−1.0 ns to attain liquid-like densities and structures at 300 K and 1 bar. Temperature and pressure were maintained using Nosé-Hoover thermostats and Hoover barostats. Production runs then took 0.6 ns with an explicit cutoff distance of 16 Å for nonbonded interactions, and long-range corrections were applied for repulsive−dispersive interactions. Electrostatic energies were calculated using the Ewald summation method with *k*-values set to 5 and $\alpha = 0.185$ Å. The structural quantities pertinent to the interpretation of the experimental solubility results were assessed through the calculation of pair radial distribution functions for selected pairs of atoms.

Results

Experimental. Liquid−liquid phase diagrams of the pyridinium-based ionic liquids plus water systems were determined in the 288.15−318.15 K temperature range at atmospheric pressure. The results are displayed in Table 1, along with their standard deviations. Due to the large differences in the molecular weight between the solute and the solvent, it is worth considering both mole and weight fraction solubilities (see, respectively, Table 1 and Supporting Information (Part 1)).

Mutual solubilities between water and $[C_4\text{-}3\text{-}C_1py][NTf_2]$ or $[C_6py][NTf_2]$ at (297 ± 1) K were previously published by Chapeaux et al.[38] For the IL-rich phase, our results deviate positively from the literature[38] by 5.91% and 0.81% for $[C_4\text{-}3\text{-}C_1py][NTf_2]$ and $[C_6py][NTf_2]$, respectively. Nevertheless, for the water-rich phase, and although the results are of the same order of magnitude, the relative deviations of our results in respect to those published by Chapeaux et al.[38] are of 6.38% and 75.36% for $[C_4\text{-}3\text{-}C_1py][NTf_2]$ and $[C_6py][NTf_2]$, respectively. Note that our mole fraction results are always greater than those presented in the literature.[38] We believe that the major deviations result from the time employed in the equilibration for both phases' separation. Chapeaux et al.[38] performed their experiments by mixing both phases during 12 h followed by 12 h of rest (for equilibrium conditions attainment). Nevertheless, we found the measurements of the ionic liquids $[C_6py][NTf_2]$ and $[C_8py][NTf_2]$ particularly difficult, and only after 48 h the equilibrium was attained; however, for the remaining ionic liquids, 24 h of equilibration was required. A general example for the time-dependent saturation conditions is presented in the Supporting Information (Part 1).

The liquid−liquid phase diagrams of all the ionic liquids studied along with that previously investigated,[39] $[C_3\text{-}3\text{-}C_1py][NTf_2]$, are depicted in Figure 2. For each set of points, homogeneous mixtures of the ionic liquid and water are found above the curves, while below them, macroscopic phase splitting occurs. The studied ionic liquids and water binary systems present thus a common upper critical solution temperature (UCST) behavior,[30,31] asymmetrically centered in the low-concentration region of the ionic liquid. It is observed that while the mole fraction solubility of the ionic liquids in water is of the order of 10^{-5} to 10^{-4} the solubility of water in the ionic liquids is much higher, in the 10^{-1} magnitude. Hence, in spite of the extreme hydrophobic nature of these ionic liquids (mainly due to the anion contribution), it is here shown that they are highly hygroscopic. Nevertheless, it should be mentioned that due to the large differences in the molecular weight between water and ionic liquids, when those values are converted to mass

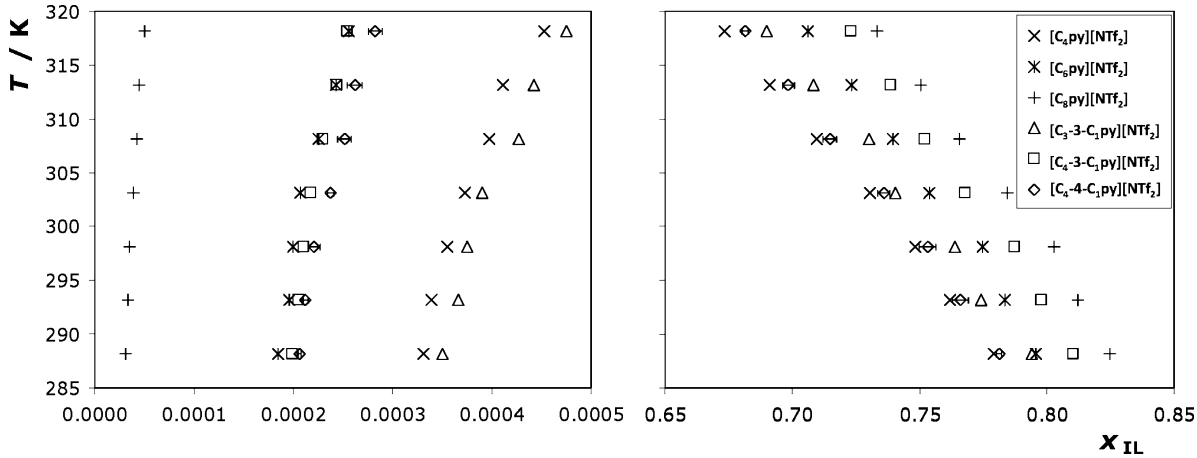

Figure 2. Temperature-phase behavior for the several studied ILs and water (left, water-rich phase; right, IL-rich phase). Standard deviations associated to the experimental measurements are presented for $[C_4\text{-}4\text{-}C_1py][NTf_2]$ as an example. Literature data,[39] triangle; all other points represent our data.

fraction compositions, the solubility of water in the IL-rich phase is only 1 order of magnitude superior to the solubility of the ionic liquid in the water-rich phase (cf. Supporting Information, Part 1).

It is well-known that the chemical and physical behavior of mixtures incorporating ionic liquids are drastically affected by the ionic liquid anion.[39] Although in a milder fashion, it is here shown that the structure of the cation also influences the liquid−liquid phase behavior of IL−water binary systems and can be used to fine-tune the phase diagrams. For instance, differences of 1 order of magnitude are observed in the water-rich phase for the solubilities of $[C_4py][NTf_2]$ and $[C_8py][NTf_2]$. The mutual miscibility of ionic liquids and water decreases with the increase in the alkyl side chain length. The surface of an ionic liquid is usually composed of hydrophobic and hydrophilic moieties, including local charges. The number of carbon atoms in the alkyl chain is one of the main factors determining the hydrophobic nature of the studied ionic liquids, and thus, assuming that there is no micelle formation or similar types of segregation (or at least, as has been found for $[C_{10}mim][NTf_2]$,[5] that we are working at saturation concentrations which are below the critical micelle concentration), the hydrophobic hydration of the ionic liquid alkyl chain controls their solubility in aqueous solution. As a matter of fact, that tendency occurs for both the monosubstituted and disubstituted ionic liquids. Nevertheless, the main goal of this work is to provide a better understanding of the structural and positional isomeric effects, and to this end, two main pairs are compared: $[C_4py][NTf_2]$ and $[C_3\text{-}3\text{-}C_1py][NTf_2]$,[39] and $[C_4\text{-}3\text{-}C_1py][NTf_2]$ and $[C_4\text{-}4\text{-}C_1py][NTf_2]$. From Figure 2, it is clear that at the water-rich phase slight deviations exist among isomers. The solubility of $[C_4py][NTf_2]$ in water is lower than that of the structural analogue $[C_3\text{-}3\text{-}C_1py][NTf_2]$. On the other hand, the solubilities of $[C_4\text{-}3\text{-}C_1py][NTf_2]$ and $[C_4\text{-}4\text{-}C_1py][NTf_2]$ are indeed similar, although the *para*-substituted ionic liquid presents a higher affinity for water. However, it is quite interesting to observe that the features of both structural and positional isomers are rather different at the IL-rich phase. Curiously, a switch in positions is observed between $[C_4py][NTf_2]$ and $[C_3\text{-}3\text{-}C_1py][NTf_2]$ at the IL-rich phase. The solubility of water in $[C_4py][NTf_2]$ is higher than the solubility of water in $[C_3\text{-}3\text{-}C_1py][NTf_2]$. Additionally, now a significant deviation is clearly observed with respect to the two positional isomers, $[C_4\text{-}3\text{-}C_1py][NTf_2]$ and $[C_4\text{-}4\text{-}C_1py][NTf_2]$. The solubility of water in $[C_4\text{-}4\text{-}C_1py][NTf_2]$ ranges between that observed for $[C_4py][NTf_2]$ and $[C_3\text{-}3\text{-}C_1py][NTf_2]$. Although larger alkyl chains are present in $[C_4\text{-}4\text{-}C_1py][NTf_2]$, the *para* substitution contributes for an enormous increment of the affinity of water to the ionic liquid. Besides the ionic liquid molecular structure, the possibility of the ionic liquid to hydrogen bond with water plays a dominant role. The alkyl simultaneous substitutions in the positions C1−C4 at the pyridinium cation lead to an enhanced distribution of charge or to a high charge density at the IL cation, when compared to the C1−C3 substitutions, favoring thus hydrogen bonding between the cations and water molecules. Moreover, the packing of water in ILs is fairly more efficient in the IL with the *para* substitutions due to a less significant steric hindrance caused by the two alkyl groups.

To describe the experimental mutual solubilities obtained, two correlations are employed. The correlations are particularly useful both to obtain the saturation values at nonworking temperatures and to determine the thermodynamic functions of solution (see discussion below). The solubility of water in the IL-rich phase is described by

$$\ln x_w = A + B/(T/\mathrm{K}) \quad (1)$$

where x_w is the mole fraction solubility of water in the IL-rich phase; T is the absolute temperature; and A and B are fitting parameters. It should be pointed out that eq 1 assumes that the molar enthalpy of solution in water, within the working temperature range, is temperature independent (B is constant).

On the other hand, the solubility of each IL in water is correlated by eq 2

$$\ln x_{IL} = C + D/(T/\mathrm{K}) + E\ln(T/\mathrm{K}) \quad (2)$$

where x_{IL} is the mole fraction solubility of an IL as a function of temperature T, and C, D, and E are the fitting parameters.

The correlation constants obtained from the fitting of the experimental data, in both rich phases, are presented in Table 2. The proposed correlations show a maximum relative deviation from experimental data of 2.34% and 2.36%, for the IL-rich (x_w) and water-rich (x_{IL}) phases, respectively. The higher relative deviations have been observed for the systems composed of $[C_6py][NTf_2]$ or $[C_8py][NTf_2]$ and water.

Aiming at exploring the molecular solvation mechanisms involved, the molar thermodynamic functions of solution are

TABLE 2: Parameters and *R*-Squared Correlations from the Fitting of the Experimental Data to Equation 1 and Equation 2 [a]

	$[C_4py][NTf_2]$	$[C_6py][NTf_2]$	$[C_8py][NTf_2]$	$[C_3\text{-}3\text{-}C_1py][NTf_2]$[39]	$[C_4\text{-}3\text{-}C_1py][NTf_2]$	$[C_4\text{-}4\text{-}C_1py][NTf_2]$
A	2.66(7)	2.33(13)	2.79(15)	2.69(14)	2.44(10)	2.52(8)
$-B$/K	1203(20)	1132(40)	1311(44)	1228(45)	1184(31)	1166(25)
R^2	0.9930	0.9969	0.9972	0.9969	0.9983	0.9988
$-C$	236(64)	254(93)	219(102)	222(77)	196(39)	167(60)
D/K	9501	10215	8155	8354	7807	6315
	(2896)	(4189)	(4597)	(3499)	(1774)	(2734)
E	34(10)	37(14)	32(15)	32(12)	28(16)	24(9)
R^2	0.9962	0.9930	0.9960	0.9965	0.9978	0.9968

[a] The values between parentheses represent the standard deviation associated with the last representative digit of each parameter.

TABLE 3: Standard Molar Thermodynamic Functions of Solution of ILs in Water at 298.15 K[a]

	$[C_4py][NTf_2]$	$[C_6py][NTf_2]$	$[C_8py][NTf_2]$	$[C_3\text{-}3\text{-}C_1py][NTf_2]$[39]	$[C_4\text{-}3\text{-}C_1py][NTf_2]$	$[C_4\text{-}4\text{-}C_1py][NTf_2]$
$\Delta_{sol}H°$	6.5(1.5)	6.9(1.5)	10.9(1.5)	6.5(1.5)	5.3(1.5)	7.2(1.5)
$\Delta_{sol}G°$	19.69(3)	21.11(1)	25.43(2)	19.56(2)	20.99(5)	20.86(7)
$-\Delta_{sol}S°$	44.2(5.1)	47.7(5.1)	48.8(5.1)	43.9(5.1)	52.7(5.2)	45.7(5.3)

[a] Units of energies in $kJ\cdot mol^{-1}$ and of entropy in $J\cdot K^{-1}\cdot mol^{-1}$. The values between parentheses represent the standard deviation associated with the last representative digit.

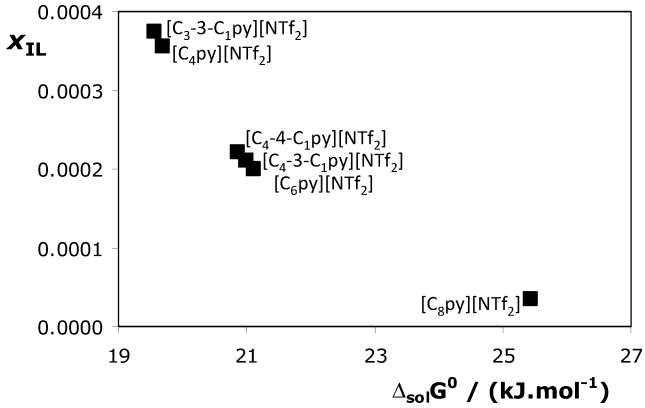

Figure 3. Mole fraction solubility of ionic liquid at the aqueous-rich phase, at 298.15 K, as a function of the respective standard molar Gibbs energy of solution.

particularly valuable. Although such properties are extremely important for molecular-based interpretations, meticulous studies on the liquid−liquid equilibria as a function of temperature are scarce.[30,31,39−45] Moreover, only molar properties of the IL-saturated solution in water can effectively be explored since only in this case one is dealing with conditions near or at infinite dilution. This is essential to ensure that no solute−solute interactions (electrostatic contribution) and/or ion pairing exist. Standard molar thermodynamic functions of the IL solutions, such as the standard molar enthalpy ($\Delta_{sol}H°$), molar Gibbs energy ($\Delta_{sol}G°$), and molar entropy ($\Delta_{sol}S°$), are given in Table 3 along with their respective standard deviations. Further details regarding their calculation can be found elsewhere.[39,40] Figure 3 plots solubility data as a function of $\Delta_{sol}G°$ and shows the internal consistency of the results.

The positive values for the enthalpies of solution indicate that the solubilization of ionic liquids in water is indeed an endothermic process, thus leading to an UCST-type of phase diagram (phase splitting as temperature decreases).[58,59] It was previously shown that the enthalpies of solution of ionic liquids in water are not significantly dependent on the cation side alkyl chain length.[40] This feature was demonstrated with imidazolium-[39,40] and pyrrolidinium-based[43] ionic liquids, combined either with hexafluorophosphate[39] or bis[(trifluoromethyl)sulfonyl]imide[40] anions. Enthalpies of solution are primarily defined by the ionic liquid anion.[39] Nevertheless, all previously studied ionic liquids[39−44] presented two or three alkyl chain substitutions at the cation, and for the disubstituted cations presented here, the same analogy is verified (after taking into account the associated standard deviations). Yet, for the monosubstituted ionic liquids studied, a significant increment on the enthalpy of solution is observed for $[C_8py][NTf_2]$. Nonetheless, such an increment on the enthalpy of solution for $[C_8py][NTf_2]$ seems to result from a higher Gibbs energy of solution. The Gibbs energy of solution reflects the energy required for the formation of a cavity (in water, in this study) capable of accommodating the ionic liquid ions—the ion solvation by water molecules. The energy required for cavity creation will certainly increase with the cation alkyl chain, but it is here shown that the Gibbs energy of solution of $[C_8py][NTf_2]$ increases twice compared to the observed increment between $[C_4py][NTf_2]$ and $[C_6py][NTf_2]$. It was also previously shown[39,40] that the entropies of solution increase approximately $-5\ J\cdot K^{-1}\cdot mol^{-1}$ per methylene addition at the ionic liquid cation, a tendency that was shown to be independent both of the cation and anion nature. Although such increment on the entropy of solution is confirmed with the disubstituted ionic liquids with the alkyl chains at C1 and C3, $[C_3\text{-}3\text{-}C_1py][NTf_2]$ and $[C_4\text{-}3\text{-}C_1py][NTf_2]$, that trend is not observed for the monosubstituted cations. For the $[C_npy][NTf_2]$ series, the increment per methylene addition ($\approx -1\ J\cdot K^{-1}\cdot mol^{-1}$) is well below that observed for the remaining ionic liquids. Taking into account that the entropic contribution controls the ionic liquid solvation in water, such smaller increments induce the small differences verified in the ionic liquid mole fraction solubilities by the addition of consecutive $-CH_2$ groups. Indeed, as shown in Figure 2, the solubilities of ionic liquids in water are less dependent on the alkyl side chain length for the $[C_npy][NTf_2]$ sequence. From these results a conclusion can be drawn: the increase on the alkyl side chain length in disubstituted cations affects much more the entropy of solution than the corresponding increase in monosubstituted cations. In addition, when changing the methyl group from the position C3 to C4, $[C_4\text{-}4\text{-}C_1py][NTf_2]$, a slight decrease in the entropies of solution occurs when compared with the positional isomer $[C_4\text{-}3\text{-}C_1py][NTf_2]$. Again, such a decrease in the entropies of solvation reflects a decrease in the ionic liquid solubility in water.

In summary, the enthalpies of solution for the ionic liquid dissolution in water do not significantly depend on the cation alkyl side chain length in disubstituted cations, while a slight dependence is verified for the monosubstituted cations. In

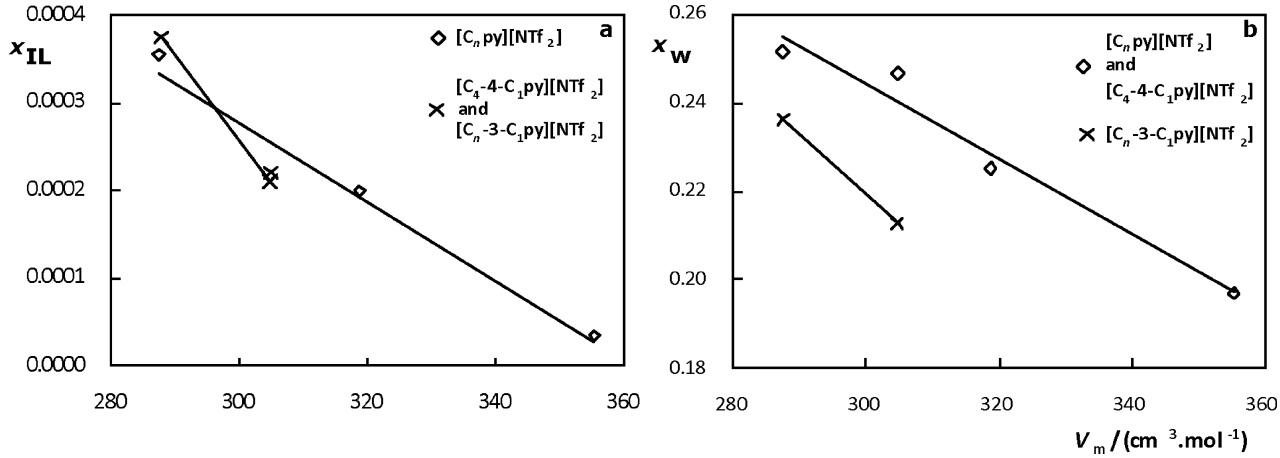

Figure 4. Mutual solubilities in the IL/water mixtures as a function of the ionic liquid molar volume. All data at 298.15 K and expressed as mole fraction of solute: (a) IL solubility, x_{IL}, in the water-rich phase; (b) water solubility, x_w, in the IL-rich phase.

addition, the decrease of the ionic liquid solubility in water is driven by the decrease in the entropies of solution. Moreover, structural and positional isomers have a different liquid−liquid phase behavior as a result of a delicate balance between energetic and entropic contributions.

The effect of the molar volume on the solubility of these ionic liquids in water and water in the ionic liquids has been investigated. The molar volumes of all studied ionic liquids were determined based on density data taken from the literature.[60] The dependence of the ionic liquid solubility in the water-rich phase and that of the water solubility in the IL-rich phase, with the ionic liquid molar volumes, are shown in Figure 4.

In Figure 4a two main trends are present: one corresponding to the monosubstituted ionic liquids and the other corresponding to the disubstituted ionic liquids. These results indicate that the ionic liquid solvation in water (in structurally analogous ionic liquids) certainly results, to a large extent, from entropic contributions ($-T\Delta_{sol}S° > \Delta_{sol}H°$). In addition, the two separate trends corroborate the distinction on entropic changes between monosubstituted and disubstituted ionic liquids (it is different to occupy the same volume at the end of an alkyl chain or at one of the positions of the pyridinium ring). These differences in the ionic liquid solvation mechanism with the number of alkyl substitutions present in the ionic liquid cation further depend on energetic contributions, which account for the different slopes of the two trends. It should be remarked that this simple approach describes quite well the experimental solubility results at the water-rich phase because it captures the key factor (entropy and its volume dependence) that rules the solvation mechanism between similar ionic liquids.

On the other hand, for the IL-rich phase (Figure 4b) two different trends are observed, one for the monosubstituted ionic liquids and the *para*-substituted cation and a different trend for the *meta*-substituted cations. Thus, the solubility of water in ionic liquids and its solvation mechanism, though still partially conditioned by entropic factors, are mainly ruled by enthalpic contributions. These will be highlighted by the results of the MD simulations discussed in the following section.

Molecular Dynamics Simulations. The mutual solubility between an ionic liquid and water is largely determined by the nature of the anions that compose the ionic fluid. Thus, one can generally speak of halogen-based ionic liquids as more "hydrophilic" than hexafluorophophate-based ones or bistriflamide-based ionic liquids as "hydrophobic". Simulation studies have confirmed this scenario by showing that, from a molecular point of view, most of the interactions in IL−water mixtures occur between the water molecules and the anions.[61]

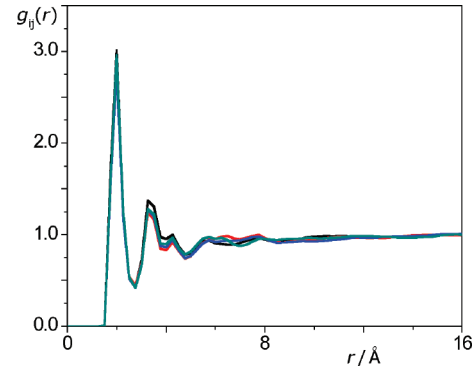

Figure 5. Anion−water radial distribution functions between the oxygen atom of water, OW, and those of $[NTf_2]^-$, OBT. All systems are composed of 40 water molecules diluted in 242 ionic liquid ion pairs. (Black line), [C_4py][NTf_2] solution; (red), [C_4-2-C_1py][NTf_2]; (blue), [C_4-3-C_1py][NTf_2]; (cyan), [C_4-4-C_1py][NTf_2].

By choosing a single anion ($[NTf_2]^-$), herein we force a situation in which the cation effect on the mutual solubility of the two components of the mixtures emerges in full, either directly via different cation−water interactions or indirectly via different anion−water interactions due to changes in the polar network caused by dissimilar interactions between the common anion and the different cations. However, water−anion radial distribution functions in the ionic liquid-rich side of the several ionic liquid solutions under discussion (Figure 5) show that in this case the interactions between water and the anions are practically constant and independent of the nature of the cation. Thus, the relative solubilities of the different ionic liquids and water will be shaped mainly by the water−cation interactions, namely, between the oxygen atom of water, OW, and the most positively charged parts of the cations—the hydrogen atoms of the aromatic ring.

Ab initio calculations of isolated $[C_4py]^+$ and $[C_4$-n-$C_1py]^+$ cations yielded point-charge distributions—from the application of the CHelpG algorithm to electron densities obtained at the MP2/cc-pVTZ(-f) level—showing that methyl substitution of the pyridinium ring at the C2 ($n = 2$, *ortho*), C3 ($n = 3$, *meta*) or C4 ($n = 4$, *para*) positions strongly affects the charge distribution in the ring (cf. Figure 6). Due to the typical resonance effects of a six-membered aromatic ring, the C2 and C4 carbons of a nonsubstituted *N*-alkylpyridinium cation will receive most of the positive charge of the nitrogen atom (Figure 6(a)). When

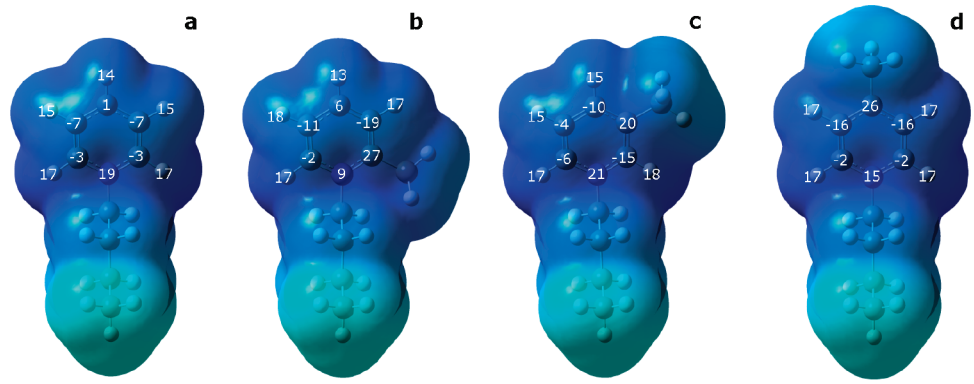

Figure 6. Electrostatic potential mapped onto an electron density isosurface (ab initio MP2/cc-pVTZ(-f)) and estimated atomic point charges (ChelpG method) on (a) *N*-butylpyridinium, (b) *N*-butyl-2-methylpyridinium, (c) *N*-butyl-3-methylpyridinium, and (d) *N*-butyl-4-methylpyridinium cations. The values superimposed on selected atoms represent the corresponding atomic point-charge densities expressed in percentage of atomic charge units (acu %). The color code represents all gradations from low positive charge densities (cyan) to high positive charge densities (dark blue). Some atomic point charges of the aromatic carbon atoms are negative.

methyl substitution takes place at one of the C2, C3, or C4 positions, the inductive effect of the methyl group causes the increase of the positive charge at that position and the reduction of the charges at the two positions adjacent to the substitution (Figure 6(b−d)). In terms of the interaction between the aromatic hydrogen atoms of the pyridinium ring and the oxygen atoms of water, the substitution effect can be summarized in the following rule-of-thumb: the more positive the charge of a given aromatic carbon, the more intense the interaction at that position between the cation and water.

It must be stressed at this point that in spite of having the most positive charge of the pyridinium ring the carbon atom where the methyl substitution takes place loses its ability to interact with water due to the loss of its aromatic hydrogen atom. Additionally it is expected that some stereochemical hindrance and charge induction effects should occur at the positions adjacent to the substitution. This state of affairs could in principle be studied using ab initio calculations between isolated cations and water molecules; however, it is more practical to model the condensed phase using MD and perform the corresponding structural analysis by representation of the pair radial distribution functions (RDFs) of the atoms involved in the solvent−solute interactions.

Several RDFs, corresponding to the correlations between the oxygen atom of water (OW) and the aromatic carbon atoms at C3 and C4 of different pyridinium cations in IL-rich solutions, are presented in Figure 7(a) (OW−C3) and Figure 7(b) (OW−C4). When the methyl substitution occurs at C2, C3, or C4, all RDFs show, as expected, a shift to longer distances of the peak corresponding to the OW−C*N* (N = 2, 3, or 4) correlation at that position (depletion of oxygen, destruction of a possible hydrogen bond) and also a decrease in intensity of the peaks of the positions adjacent to the substituted carbon atom (no shift but decrease in intensity).

Figure 8 shows the combination of the two effects caused by the methylation of a given position of the pyridinium ring−charge changes and position blockage acting simultaneously. Each panel of the figure depicts RDFs corresponding to the correlations between the oxygen atom of water (OW) and the aromatic hydrogen atoms (H*N*) of unmethylated and methylated pyridinium cations contained in IL-rich solutions. Each set of RDFs is also accompanied by a schematic figure that shows the charge distribution and position blockage in each type of pyridinium ring. Both representations−the schematic figures are based on charge distributions and induction effects calculated ab initio, and the RDFs are calculated from the MD

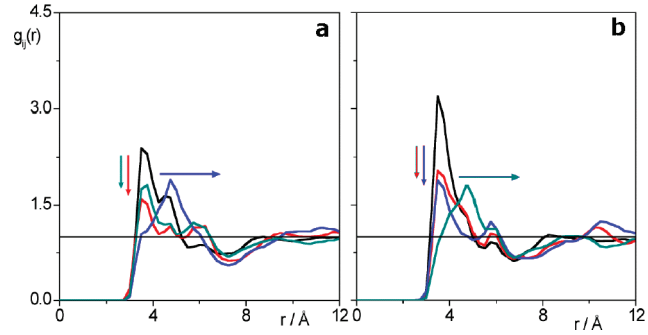

Figure 7. Site−site radial distribution functions of water diluted in $[C_4py][NTf_2]$ (black), $[C_4\text{-}2\text{-}C_1py][NTf_2]$ (blue), $[C_4\text{-}3\text{-}C_1py][NTf_2]$ (red), and $[C_4\text{-}4\text{-}C_1py][NTf_2]$ (cyan). (a) C3−OW sites and (b) C4−OW sites. The arrows indicate either the elimination of the aromatic hydrogen−OW interaction at the substituted position (right shift) or the hindrance of that interaction at the adjacent positions (down shifts).

simulation data−not only convey self-consistent information but also can help explain the observed solubility trends in the IL-rich solutions.

The solubility of water in $[C_4py][NTf_2]$ is mainly due to the interactions between OW and the aromatic hydrogens at the *ortho* and *para* positions that are attached to the C2 and C4 carbon atoms (cf. Figure 8(a)). When methylation occurs at the *para* position, as in the case of the $[C_4\text{-}4\text{-}C_1py][NTf_2]$ IL, the solubility of water only decreases marginally because the two *ortho* hydrogens are not affected by the *para* substitution and, in fact, are able to compensate the loss of the hydrogen at the *para* position (cf. the charge changes at the *ortho* positions in Figure 8(a) and (d)). On the other hand, methylation in the *meta* position (leading to $[C_4\text{-}3\text{-}C_1py][NTf_2]$) hinders the interactions at the adjacent *para* and *ortho* positions, leaving just one available "strong" *ortho* hydrogen to interact with water (cf. Figure 8(c)). The solubility of water in the ionic liquid is strongly decreased in this case.

Therefore, the solubility of water in $[C_npy][NTf_2]$, $[C_n\text{-}3\text{-}C_1py][NTf_2]$, and $[C_4\text{-}4\text{-}C_1py][NTf_2]$ ionic liquids can be understood at a molecular level taking into account different pieces of information gathered using ab initio or MD techniques providing an explanation for the observations reported in Figure 4b.

As mentioned before, the solubility of the ionic liquids in the water-rich media is controlled by entropic factors: water has to accommodate ions that have a rather large organic part, which implies the usual hydrophobic effect. The larger the

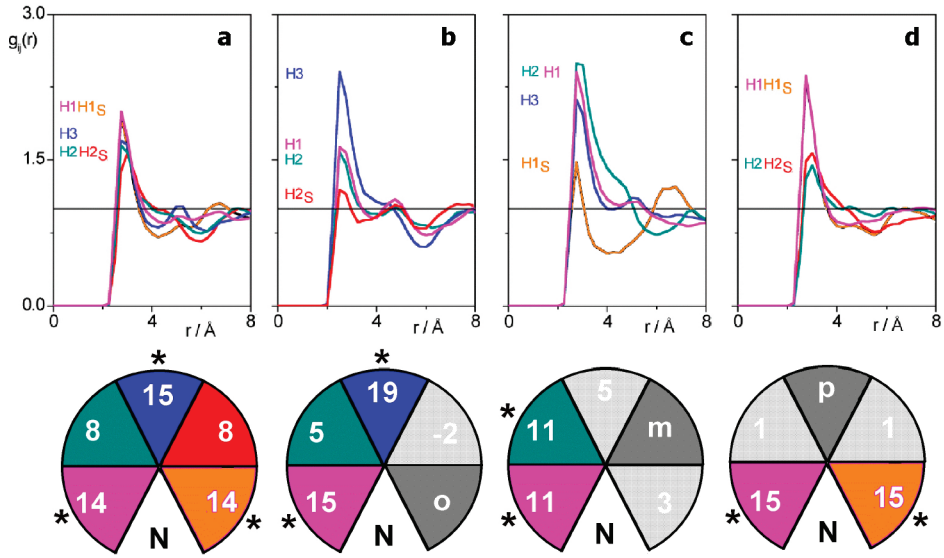

Figure 8. Top panels: Site−site radial distribution functions of water diluted in [C_4py][NTf_2] (a), [C_4-2-C_1py][NTf_2] (b), [C_4-3-C_1py][NTf_2] (c), and [C_4-4-C_1py][NTf_2] (d). H*N*−OW ($N = 1$, 1S, 2, 2S, or 3) interactions are labeled and ordered directly in the graphs. Bottom panels: schematic representation of the pyridinium ring highlighting the positions (*) that perform stronger interactions with water. The numbers represent the atomic point charges (acu %) attributed to each sector of the ring; "o", "m", and "p" represent the methylated 2 (*ortho*), 3 (*meta*), and 4 (*para*) positions, respectively. Dark gray positions are not capable of interactions with OW due to methyl substitution; the corresponding adjacent positions (in light gray) are hindered.

organic part of a given ionic liquid ion, the larger such an effect, which means that cations with longer alkyl side chains will have lower solubilities in water. It is also obvious that methyl substitution in the alkyl side chain is not the same as methyl substitution in the pyridinium ring: the former substitution increases the nonpolar part of the cation, and the latter does not; instead, it affects the way water molecules solvate the polar head of the cation. This explains the different trends found in Figure 4a. MD simulations performed in water-rich solutions have indeed demonstrated that the water molecules are able to solvate both the anion (mainly through hydrogen bonds between the oxygen atoms of the $[NTf_2]^-$ anion and the hydrogen atoms of water) and the pyridinium ring of the cation (via the interactions described in the previous paragraphs). The simulations have also shown that when the amount of ion pairs is larger than one (in simulations with 3000 water molecules) the ionic liquid ions tend to aggregate, confirming their strong tendency to form a second phase.

While the solubility of similar ionic liquids in water is entropically driven, as discussed above, the solvation process of water in the IL-rich solutions is of a completely different nature. In spite of their label of "hydrophobic" ionic liquids, bistriflamide-based ionic liquids are in fact hygroscopic—they are able to incorporate in their midst quite a substantial amount of water molecules (especially if we tally them in terms of mole fraction). From the molecular and structural points of view the picture is quite simple: ionic liquids are nanosegregated fluids with a polar network permeated by nonpolar domains. The former regions have quite high-charge (positive and negative) densities and interact mainly through electrostatic forces. Water is "solvated" in these regions of the ionic liquid, and the amount of water tolerated depends mainly on the ability of the ionic fluid to incorporate it near its polar network without disrupting it. Ionic liquids with larger nonpolar domains will exhibit polar networks that are already "overstretched" and are thus unable to solvate large amounts of water. That is the reason why, even when expressed in mole fraction, the solubility of water in [$C_n$py][NTf_2] decreases as n increases. The ability of water to interact with the ions (or parts of them that are included in the polar network) is also important (in fact, it is the ability to interact with the anion that matters most). We have seen (Figure 4b) that the solubility of water in [C_4-4-C_1py][NTf_2] is almost the same as that of [C_4py][NTf_2]. It does not matter that [C_4-4-C_1py][NTf_2] is bulkier than [C_4py][NTf_2]: only the fact that water is able to interact in a similar way with the two cations is relevant. On the other hand, in ionic liquids of the type [C_n-3-C_1py][NTf_2] the water−cation interactions are weaker, and the resulting water solubility is smaller.

Conclusions

The development of a molecular-based understanding of the liquid−liquid phase equilibria in (water + ionic liquids) mixtures is of great importance. This work reports new data for the mutual solubilities between several isomeric pyridinium-based ionic liquids and water in the 288.15−318.15 K temperature range. The main focus was to analyze the effect of structural changes on the cation of a given ionic liquid, namely, its alkyl side chain length and its structural and positional isomerism. It was found that an increase in the cation side alkyl chain leads to a decrease in the mutual solubility of the studied ionic liquid with water—increase of the ionic liquid hydrophobic character—while the presence of distinct isomers of the ionic liquid has different effects both on the solubility of the ionic liquid in water and on that of water in IL-rich solutions. The explicit consideration of the role of isomeric forms of a given ionic liquid in the fluid phase behavior of liquid binary systems is very rarely investigated.

The temperature dependence of the solubility data allowed us to estimate the corresponding standard molar thermodynamic functions of solution. The molar enthalpies of solution showed to be almost independent of the alkyl side chain length for the alkyl-disubstituted ILs, whereas a small dependence was found for the [$C_n$py][NTf_2] ionic liquids. Generally, the very low solubility of these ionic liquids in water is determined by both the extreme loss of entropy upon dilution ($-T\cdot\Delta_{sol}S^\circ \sim 2/3\cdot\Delta_{sol}G^\circ > 0$) and the endothermic nature ($\Delta_{sol}H^\circ \sim 1/3\cdot\Delta_{sol}G^\circ > 0$) of the mixing. Quantitative correlations have been established between the solubility of the ionic liquids at

the water-rich phase and their molar volumes, corroborating the fact that the dissolution process in water is essentially entropically driven and largely depends on the solute size.

On the other hand, molecular simulations allowed us to interpret correctly the dissolution of water in the ionic liquid media, at the other side of the immiscibility envelope. In this case, charge distribution and structure shifts caused by the methylation of the pyridinium ring are responsible for the observed solubility changes among *N*-alkylpyridinium-based ILs and their *meta*- and *para*-methylated counterparts.

Acknowledgment. The authors thank FC&T for Project PTDC/EQU-FTT/65252/2006. MGF, CMSSN, KS, and CB acknowledge grants SFRH/BPD/41781/2007, SFRH/BD/70641/2010, SFRH/BPD/38339/2007, and SFRH/BPD/43346/2008, respectively.

Supporting Information Available: Part 1: ^{1}H, ^{13}C, and ^{19}F NMR spectra for the studied ILs, solubility dependence on time of equilibration, and mass fraction compositions for the mutual solubilities between ILs and water. Part 2: Force field parametrization for the bistriflamide and alkylpyridinium ions and water molecules included in the MD simulations. This material is available free of charge via the Internet at http://pubs.acs.org.

References and Notes

(1) Seddon, K. R. *Nat. Mater.* **2003**, *2*, 363.
(2) Earle, M. J.; Esperança, J. M. S. S.; Gilea, M. A.; Canongia Lopes, J. N.; Rebelo, L. P. N.; Magee, J. W.; Seddon, K. R.; Widegren, J. A. *Nature* **2006**, *439*, 831.
(3) Santos, L. M. N. B. F.; Canongia Lopes, J. N.; Coutinho, J. A. P.; Esperança, J. M. S. S.; Gomes, L. R.; Marrucho, I. M.; Rebelo, L. P. N. *J. Am. Chem. Soc.* **2007**, *129*, 284.
(4) Esperança, J. M. S. S.; Canongia Lopes, J. N.; Tariq, M.; Santos, L. M. N. B. F.; Magee, J. W.; Rebelo, L. P. N. *J. Chem. Eng. Data* **2010**, *55*, 3.
(5) Blesic, M.; Marques, M. H.; Plechkova, N. V.; Seddon, K. R.; Rebelo, L. P. N.; Lopes, A. *Green Chem.* **2007**, *9*, 481.
(6) Hardacre, C.; Holbrey, J. D.; McMath, S. E. J.; Bowron, D. T.; Soper, A. K. *J. Chem. Phys.* **2003**, *118*, 273.
(7) Triolo, A.; Mandanici, A.; Russina, O.; Rodriguez-Mora, V.; Cutroni, M.; Hardacre, C.; Bleif, H.-J.; Keller, L.; Ramos, M. A. *J. Phys. Chem. B* **2006**, *110*, 21357.
(8) Wang, Y.; Voth, G. A. *J. Am. Chem. Soc.* **2005**, *127*, 12192.
(9) Canongia Lopes, J. N.; Pádua, A. A. H. *J. Phys. Chem. B* **2006**, *110*, 3330.
(10) Rebelo, L. P. N.; Canongia Lopes, J. N.; Esperança, J. M. S. S.; Guedes, H. J. R.; Łachwa, J.; Najdanovic-Visak, V.; Visak, Z. P. *Acc. Chem. Res.* **2007**, *40*, 1114.
(11) Cammarata, L.; Kazarian, S. G.; Salter, P. A.; Welton, T. *Phys. Chem. Chem. Phys.* **2001**, *3*, 5192.
(12) Umebayashi, Y.; Jiang, J.-C.; Lin, K.-H.; Shan, Y.-L.; Fujii, K.; Seki, S.; Ishiguro, S.-I.; Lin, S. H.; Chang, H.-C. *J. Chem. Phys.* **2009**, *131*, 234502.
(13) Gao, Y.; Li, N.; Zheng, L.; Bai, X.; Yu, L.; Zhao, X.; Zhang, J.; Zhao, M.; Li, Z. *J. Phys. Chem. B* **2007**, *111*, 2506.
(14) Zhang, L.; Xu, Z.; Wang, Y.; Li, H. *J. Phys. Chem. B* **2008**, *112*, 6411.
(15) Mele, A.; Trans, C. D.; Lacerda, S. H. D. *Angew. Chem., Int. Ed.* **2003**, *42*, 4364.
(16) Singh, T.; Kumar, A. *J. Phys. Chem. B* **2007**, *111*, 7843.
(17) Zhu, X.; Wang, Y.; Li, H. *AIChE J.* **2008**, *55*, 198.
(18) Moreno, M.; Castiglione, F.; Mele, A.; Pasqui, C.; Raos, G. *J. Phys. Chem. B* **2008**, *112*, 7826.
(19) Freire, M. G.; Neves, C. M. S. S.; Silva, A. M. S.; Santos, L. M. N. B. F.; Marrucho, I. M.; Rebelo, L. P. N.; Shah, J. K.; Maginn, E. J.; Coutinho, J. A. P. *J. Phys. Chem. B* **2010**, *114*, 2004.
(20) Rivera-Ruvero, S.; Baldelli, S. *J. Phys. Chem. B* **2006**, *110*, 15499.
(21) Saha, S.; Hamaguchi, H.-O. *J. Phys. Chem. B* **2006**, *110*, 2777.
(22) Miki, K.; Westh, P.; Nishikawa, K.; Koga, Y. *J. Phys. Chem. B* **2005**, *109*, 9014.
(23) Li, W.; Zhang, Z.; Han, B.; Hu, S.; Xie, Y.; Yang, G. *J. Phys. Chem. B* **2007**, *111*, 6452.
(24) Hanke, C. G.; Lynden-Bell, R. M. *J. Phys. Chem. B* **2003**, *107*, 10873.
(25) Kelkar, M. S.; Maginn, E. J. *J. Phys. Chem. B* **2007**, *111*, 4867.
(26) Raju, S. G.; Balasubramanian, S. *J. Phys. Chem. B* **2009**, *113*, 4799.
(27) Anthony, J. L.; Maginn, E. J.; Brennecke, J. F. *J. Phys. Chem. B* **2001**, *105*, 10942.
(28) Wong, D. S. H.; Chen, J. P.; Chang, J. M.; Chou, C. H. *Fluid Phase Equilib.* **2002**, *194*−*197*, 1089.
(29) Crosthwaite, J. M.; Aki, S. N. V. K.; Maginn, E. J.; Brennecke, J. F. *J. Phys. Chem. B* **2004**, *108*, 5113.
(30) Rebelo, L. P. N.; Najdanovic-Visak, V.; Visak, Z. P.; Ponte, M. N.; Szydlowski, J.; Cerdeirina, C. A.; Troncoso, J.; Romani, L.; Esperança, J. M. S. S.; Guedes, H. J. R.; Sousa, H. C. *Green Chem.* **2004**, *6*, 369.
(31) Najdanovic-Visak, V.; Esperança, J. M. S. S.; Rebelo, L. P. N.; Ponte, M. N.; Guedes, H. J. R.; Seddon, K. R.; Szydlowski, J. *Phys. Chem. Chem. Phys.* **2002**, *4*, 1701.
(32) Alfassi, Z. B.; Huie, R. E.; Milman, B. L.; Neta, P. *Anal. Bioanal. Chem.* **2003**, *377*, 159.
(33) Shvedene, N. V.; Borovskaya, S. V.; Sviridov, V. V.; Ismailova, E. R.; Pletnev, I. V. *Anal. Bioanal. Chem.* **2005**, *381*, 427.
(34) Papaiconomou, N.; Yakelis, N.; Salminen, J.; Bergman, R.; Prausnitz, J. M. *J. Chem. Eng. Data* **2006**, *51*, 1389.
(35) Domańska, U.; Marciniak, A. *Green Chem.* **2007**, *9*, 262.
(36) Domańska, U.; Bakala, I.; Pernak, J. *J. Chem. Eng. Data* **2007**, *52*, 309.
(37) Papaiconomou, N.; Salminen, J.; Lee, J. M.; Prausnitz, J. M. *J. Chem. Eng. Data* **2007**, *52*, 833.
(38) Chapeaux, A.; Simoni, L. D.; Stadtherr, M. A.; Brennecke, J. F. *J. Chem. Eng. Data* **2007**, *52*, 2462–2467.
(39) Freire, M. G.; Neves, C. M. S. S.; Carvalho, P. J.; Gardas, R. L.; Fernandes, A. M.; Marrucho, I. M.; Santos, L. M. N.B. F.; Coutinho, J. A. P. *J. Phys. Chem. B* **2007**, *111*, 13082.
(40) Freire, M. G.; Carvalho, P. J.; Gardas, R. L.; Marrucho, I. M.; Santos, L. M. N. B. F.; Coutinho, J. A. P. *J. Phys. Chem. B* **2008**, *112*, 1604.
(41) Freire, M. G.; Carvalho, P. J.; Gardas, R. L.; Santos, L. M. N. B. F.; Marrucho, I. M.; Coutinho, J. A. P. *J. Chem. Eng. Data* **2008**, *53*, 2378.
(42) Freire, M. G.; Carvalho, P. J.; Silva, A. M. S.; Santos, L. M. N. B. F.; Rebelo, L. P. N.; Marrucho, I. M.; Coutinho, J. A. P. *J. Phys. Chem. B* **2009**, *113*, 202.
(43) Freire, M. G.; Neves, C. M. S. S.; Ventura, S. P. M.; Pratas, M. J.; Marrucho, I. M.; Oliveira, J.; Coutinho, J. A. P.; Fernandes, A. M. *Fluid Phase Equilib.* **2010**, *294*, 234.
(44) Neves, C. M. S. S.; Batista, M. L. S.; Cláudio, A. F. M.; Santos, L. M. N. B. F.; Marrucho, I. M.; Freire, M. G.; Coutinho, J. A. P. *J. Chem. Eng. Data* **2010**, DOI: 10.1021/je100638g.
(45) Letcher, T. M.; Ramjugernath, D.; Tumba, K.; Królikowski, M.; Domańska, U. *Fluid Phase Equilib.* **2010**, *294*, 89.
(46) Dreiseitlová, J.; Řehák, K.; Vreekamp, R. *J. Chem. Eng. Data* **2010**, *55*, 3051.
(47) Docherty, K. M.; Dixon, J. K.; Kulpa Jr, C. F. *Biodegradation* **2007**, *18*, 481.
(48) Harjani, J. R.; Singer, R. D.; Garcia, M. T.; Scammells, P. J. *Green Chem.* **2008**, *10*, 436.
(49) Harjani, J. R.; Singer, R. D.; Garcia, M. T.; Scammells, P. J. *Green Chem.* **2009**, *11*, 83.
(50) Smith, W.; Forester, T. R. *The DL_POLY Package of Molecular Simulation Routines (v.2.17). The Council for The Central Laboratory of Research Councils*; Daresbury Laboratory: Warrington, 2006.
(51) Canongia Lopes, J. N.; Pádua, A. A. H. *J. Phys. Chem. B* **2004**, *108*, 16893.
(52) Canongia Lopes, J. N.; Pádua, A. A. H. *J. Phys. Chem. B* **2006**, *110*, 19586.
(53) Frisch, M. J.; Trucks, G. W.; Schlegel, H. B.; Scuseria, G. E.; Robb, M. A.; Cheeseman, J. R.; Montgomery, J. A., Jr.; Vreven, T.; Kudin, K. N.; Burant, J. C.; Millam, J. M.; Iyengar, S. S.; Tomasi, J.; Barone, V.; Mennucci, B.; Cossi, M.; Scalmani, G.; Rega, N.; Petersson, G. A.; Nakatsuji, H.; Hada, M.; Ehara, M.; Toyota, K.; Fukuda, R.; Hasegawa, J.; Ishida, M.; Nakajima, T.; Honda, Y.; Kitao, O.; Nakai, H.; Klene, M.; Li, X.; Knox, J. E.; Hratchian, H. P.; Cross, J. B.; Bakken, V.; Adamo, C.; Jaramillo, J.; Gomperts, R.; Stratmann, R. E.; Yazyev, O.; Austin, A. J.; Cammi, R.; Pomelli, C.; Ochterski, J. W.; Ayala, P. Y.; Morokuma, K.; Voth, G. A.; Salvador, P.; Dannenberg, J. J.; Zakrzewski, V. G.; Dapprich, S.; Daniels, A. D.; Strain, M. C.; Farkas, O.; Malick, D. K.; Rabuck, A. D.; Raghavachari, K.; Foresman, J. B.; Ortiz, J. V.; Cui, Q.; Baboul, A. G.; Clifford, S.; Cioslowski, J.; Stefanov, B. B.; Liu, G.; Liashenko, A.; Piskorz, P.; Komaromi, I.; Martin, R. L.; Fox, D. J.; Keith, T.; Al.Laham, M. A.; Peng, C. Y.; Nanayakkara, A.; Challacombe, M.; Gill, P. M. W.; Johnson, B.; Chen, W.; Wong, M. W.; Gonzalez, C.; Pople, J. A. *Gaussian 03*, revision C.05; Gaussian, Inc: Wallingford, CT, 2004.
(54) Jorgensen, W. L.; Maxwell, D. S.; Tirado-Rives, J. *J. Am. Chem. Soc.* **1996**, *118*, 11225.
(55) Kaminski, G.; Jorgensen, W. L. *J. Phys. Chem.* **1996**, *100*, 18010.

(56) McDonald, N. A.; Jorgensen, W. L. *J. Phys. Chem. B* **1998**, *102*, 8049.
(57) Praprotnik, M.; Janežič, D.; Mavri, J. *J. Phys. Chem. A* **2004**, *108*, 11056.
(58) Rebelo, L. P. N. *Phys. Chem. Chem. Phys.* **1999**, *1*, 4277.
(59) Rebelo, L. P. N.; Sousa, H. C. *J. Polym. Sci., Part B* **2000**, *38*, 632.
(60) Oliveira, F. S.; Freire, M. G.; Carvalho, P. J.; Coutinho, J. A. P.; Canongia Lopes, J. N.; Rebelo, L. P. N.; Marrucho, I. M. *J. Chem. Eng. Data* **2010**, *55*, 4514.
(61) Canongia Lopes, J. N.; Costa Gomes, M. F.; Pádua, A. A. H. *J. Phys. Chem. B* **2006**, *110*, 16816.

JP1093788